JSR Publications

Available Online

J. Sci. Res. **17** (1), 151-163 (2025)

JOURNAL OF SCIENTIFIC RESEARCH

www.banglajol.info/index.php/JSR

Molecular Docking, Electronic Properties, Quantum Chemical Analysis (PES, MEP, HOMO–LUMO, FMO, NLO) and Spectroscopic (FT–IR, FT–RAMAN, UV–Vis–NIR) Investigations of Quinoxaline

G. Anand[1*], M. Sivasubramanian[2], I. Manimehan[1], P. Jagdish[2], P. Paramasivam[2], R.K. Asmitha[3]

[1]Department of Physics, M.R. Government Arts College (Affiliated to Bharathidasan University, Tiruchirappalli), Mannargudi, India–614 001

[2]Department of Physics, Rajah Serfoji Government College (Affiliated to Bharathidasan University, Tiruchirappalli), Thanjavur, India–613 005

[3]Department of Physics, Bon Secours Arts and Science College for Women (Affiliated to Bharathidasan University, Tiruchirappalli), Mannargudi, India–614 001

Received 18 August 2024, accepted in final revised form 29 September 2024

Abstract

Vibrational and electronic analyses were conducted for quinoxaline utilizing FT-IR, FT – Raman, and UV–Vis–NIR techniques. Infrared intensities, Raman scattering data, vibrational wavenumbers, molecular geometry, and optimal structure were determined using the Density Functional Theory/ Becke's three-parameter exchange functional with the Lee-Yang-Parr correlation functional (DFT/B3LYP) method with a 6–31G** basis set. Electron localization and delocalization were examined through highest occupied molecular orbital and lowest unoccupied molecular orbital (HOMO–LUMO) analysis, while Molecular Electrostatic Potential (MEP) analyses were undertaken to identify potential electrophilic, nucleophilic, and radical attacks. The electron affinity, electronegativity, chemical potential, ionization potential, electrophilicity and hardness, softness, stability of the compound were characterized via FMO (Frontier Molecular Orbital) studies. Nonlinear optical (NLO) characterizations involved the determination of dipole moment, polarizability, and first–order hyperpolarizability. Additionally, Molecular Docking analysis of quinoxaline was carried out to know its binding orientation, affinity, and activity.

Keywords: DFT; MEP; FMO; Hyperpolarizability; Molecular docking.

doi: https://dx.doi.org/10.3329/jsr.v17i1.74446 J. Sci. Res. **17** (1), 151-163 (2025)

1. Introduction

Quinoxaline, with the molecular formula C8H6N2, is a significant nitrogen–containing heterocyclic compound formed by the fusion of two aromatic rings, benzene, and pyrazine, hence also referred to as benzopyrazine [1]. This low melting point, white crystalline

* *Corresponding author*: geayea21@gmail.com

powder is soluble in water and melts just above room temperature at 32 °C. In the medical field, quinoxaline compounds have numerous applications, including anticancer, anti–inflammatory, antiviral, anti–diabetic, antimalarial, antiprotozoal, and antibacterial activities [2-8]. Beyond medicine, quinoxaline and its derivatives find applications in various fields such as the dye industry, electroluminescent materials, organic semiconductors, organic light–emitting devices, and semiconducting devices [9-11].

The promising biological activity and therapeutic applications of quinoxaline have spurred interest among researchers to synthesize derivatives. Antibiotics like olaquindox, carbadox, echinomycin, levomycin, which are active against several transplantable tumors, are derived from quinoxaline [12]. Subsequent characterizations aim to establish the properties of these derivatives for improved applications. The structural nucleus of quinoxaline, particularly the atoms S and N, plays a pivotal role in deriving a large number of new compounds and their diverse applications [12-14], mainly through the replacement of one or more carbon atoms of the naphthalene ring.

While quinoxaline has been extensively studied for its potential medical applications, a comprehensive quantum chemical and experimental analysis of quinoxaline has not been undertaken to a significant extent. Given the wide range of applications of this compound, it is imperative to analyze its characteristics thoroughly. In this study, spectroscopic characterizations were performed using FT–IR, FT–Raman, and Ultra Violet techniques (UV). Quantum chemical calculations were conducted using the Density Functional Theory (DFT) method with the B3LYP functional and a 6–31G** basis set. Experimental values were compared with theoretical calculations after appropriate scaling. Electrophilic, nucleophilic, and radical attacks were investigated using Molecular Electrostatic Potential (MEP) and contour surface analysis. The chemical and kinetic stabilities were characterized through FMO studies, while highest occupied molecular orbital and lowest unoccupied molecular orbital (HOMO–LUMO) energy gap analysis provided insights into the chemical hardness and softness of the molecule. NLO properties were studied by determining the dipole moment, polarizability, and first–order hyperpolarizability. Furthermore, the biological activity of the molecule, ligand interactions with proteins, and binding energy were investigated through molecular docking studies.

2. Experimental Details

The compound under investigation, quinoxaline (purity: 99 %), was obtained from Sigma Aldrich and used in its original form for experimental purposes. It underwent FT–IR, FT–Raman, and UV–Vis–NIR tests. FT–IR spectral measurements of quinoxaline were conducted in the range of 4000–400 cm^{-1} at room temperature using a BRUKER IFS 66V FT–IR spectrometer employing the KBr pellet technique. FT–Raman spectra were obtained using a Bruker RFS 27 FT Raman spectrometer, utilizing a Nd:YAG laser as the excitation source, covering the range of 4000–50 cm^{-1} at a spectral resolution of 0.8 to 4 cm^{-1}, also at room temperature. The electronic spectrum was recorded at room temperature using a Perkin Elmer UV spectrometer, spanning the range of 200 nm to 800 nm.

3. Computational Details

The initial geometry of quinoxaline was entirely optimized using the B3LYP method with a 6–31G** basis set, incorporated into the Gaussian 09W package [15,16]. This method combines Becke's three–parameter hybrid functional with the Lee–Yang–Parr correlation functional (B3LYP) [17,18]. Energy calculations were conducted for potential conformers, and vibrational wavenumbers with potential energy distribution (PED) were computed using the VEDA 4.0 program [19]. The resulting harmonic vibrational frequencies were scaled by a factor of 0.9614 [20] to achieve suitable agreement with experimental data.

Molecular electrostatic potentials (MEP), electronic properties, HOMO–LUMO, and Frontier Molecular Orbitals (FMO) [21] were computed at the B3LYP level with the 6–31G** basis set. NLO characterization was performed by calculating polarizability and hyperpolarizability. To determine the ideal binding orientation and affinity, molecular docking analysis was conducted using the automated docking software Auto Dock [22].

4. Results and Discussion

4.1. *Molecular geometry*

The Potential Energy Scan analysis of quinoxaline revealed a single conformer with energy of 310.7838 kJ/mol, attributed to the absence of rotatable bonds, and is depicted in figure 1. DFT calculations were conducted using Gaussian 09W [15] with the B3LYP/6–31G** basis set. Quantum chemical calculations are typically performed within a finite set of basis functions. In these cases, the wave functions under consideration are all represented as vectors, the components of which correspond to coefficients in a linear combination of the basis functions in the basis set used. The operators are then represented as matrices, in this finite basis. When molecular calculations are performed, it is common to use basis composed of a finite number of atomic orbitals, centered at each atomic nucleus within the molecule.

Initially, these atomic orbitals were typically Slater orbital, which corresponded to a set of functions which decayed exponentially with distance from the nuclei. It is easier to calculate overlap and other integrals with Gaussian basis functions and this led to huge computational savings of the many basis sets composed of Gaussian – type orbitals (GTOs), the smallest are called minimal basis sets and they typically composed of the minimum number of basis functions required to represent all of the electrons on each atom.

The most common addition to minimal basic sets is the addition of polarization functions, denoted by an asterisk (*). Two asterisks (**), indicate that polarization function is also added to light atoms (hydrogen and helium). These additional basis functions can be important when considering anions and other large, soft molecular system [23].

Table 1 presents the optimized bond lengths, bond angles, and their averages for the quinoxaline molecule. In its optimized geometric structure, the molecule features six C–H bonds with an average length of 1.086643 Å, four C–N bonds averaging 1.340739 Å, and five C–C bonds with an average length of 1.4016966 Å. Notably, C–H bonds are the shortest

while C–C bonds are the longest, attributed to the greater bond length of homonuclear C–C bonds compared to hetero nuclear C–H and C–N bonds [24]. The bond angles range from a minimum of 116.23° for C3–N4–C5 and C2–N1–C10 bonds to a maximum of 122.19° for the H13–C6–C7 bond. The bond angles are identical between H11–C2–N1and H12–C3–N4 and is 117.39º and the angle between N1–C10–C9 and N4–C5–C6 are also identical of 119.49º.

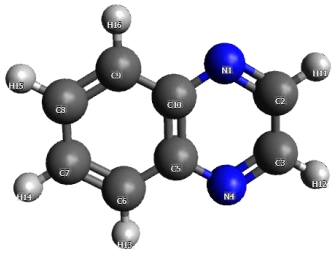

Fig. 1. Conformer of quinoxaline.

Table 1. Molecular Geometry of quinoxaline.

Parameters	Bond length (Å)	Parameters	Bond angle (º)
	Based on DFT calculations		Based on DFT calculations
C2–H11	1.088953	C3–N4–C5	116.23
C3–H12	1.088953	C2–N1–C10	116.23
C6–H13	1.085094	C10–C9–C8	119.93
C7–H14	1.085883	C7–C6–C5	119.93
C8–H15	1.085882	C9–C8–C7	120.68
C9–H16	1.085094	C8–C7–C6	120.68
N1–C2	1.316326	H11–C2–N1	117.39
N4–C3	1.316325	H12–C3–N4	117.39
N1–C10	1.365154	H14–C7–C8	119.31
N4–C5	1.365154	H15–C8–C9	120.02
C7–C6	1.376625	H16–C9–C10	117.88
C9–C8	1.376625	H13–C6–C7	122.19
C6–C5	1.418278	N1–C10–C9	119.49
C8–C7	1.418677	N4–C5–C6	119.49
C10–C9	1.418278		

4.2. *Molecular vibrations and stimulated spectra*

Regarding molecular vibrations and stimulated spectra, quinoxaline belongs to the C1 point group symmetry and comprises 16 atoms with 68 electrons. It possesses 42 fundamental modes of vibrations, including 29 in–plane and 13 out–of–plane vibrations, all of which are IR and Raman active. Vibrational frequencies were calculated at the B3LYP level with a 6–31G** basis set, scaled by a factor of 0.9614, and assignments were made based on experimentally observed FTIR and FT–Raman spectra using the VEDA program. The molecule exhibits aromatic and aliphatic C–H stretching, C–C, C=C, C–N stretching vibrations and C–N–C, C–C–N, H–C–C bending mode vibrations. The IR intensity and Raman activity and vibrational assignments were tabulated in Table 2. The comparative

experimental and theoretical IR and Raman spectra are shown in Figs. 2 and 3. There is a good agreement between calculated and observed vibrational modes [25,26]

Table 2. Calculated frequencies and vibrational assignments of quinoxaline based on B3LYP/6–31G** DFT calculation.

Mode No.	Observed frequencies		Calculated Frequencies (Scaled)	Reduced mass	Force constant	IR Intensity	Raman activity	Assignments
	IR	Raman						
1.	–	–	175	4.1897	0.0765	0.0000	0.4739	N1-C5-C9-C10 (Wagging)
2.	–	189	185	4.2149	0.0858	4.2793	0.0059	N4-C6-C10-C5 (Wagging)
3.	–	400	397	4.7531	0.4435	4.3100	0.0555	C8-C7-C6-C5 (Torsional)
4.	–	–	415	4.6672	0.4753	9.7306	4.8310	C9-C8-C7-C6 (Torsional)
5.	–	–	480	3.0473	0.4139	0.0000	0.9095	C10-C9-C8-C7 (Torsional)
6.	–	–	502	4.0065	0.5962	0.2447	0.1213	C3-N4-C5-C6 (Torsional)
7.	532	528	535	7.4871	1.2639	0.0020	12.0759	C2-N1-C10 (Bending)
8.	–	–	544	7.1685	1.2526	0.2975	8.9645	C10-C9-C8 (Bending)
9.	601	–	615	8.5098	1.9003	2.5937	0.2178	C2-N1-C10-C5 (Torsional)
10.	–	–	653	3.5268	0.8865	0.0000	0.7269	C8-C7-C6 (Bending)
11.	751	755	773	5.6276	1.9817	4.3574	33.6318	C9-C8-C7 (Bending)
12.	–	–	778	1.2517	0.4468	45.7095	4.3890	H16-C9-C10-C5 (Torsional)
13.	–	–	814	3.0895	1.2074	0.0000	3.0158	H12-C3-N4-C5 (Torsional)
14.	864	–	849	5.7815	2.4590	0.9750	0.1364	H15-C8-C9-C10 (Torsional)
15.	–	–	888	1.2204	0.5674	19.2787	1.2820	C3-N4-C5 (Bending)
16.	–	–	896	1.7924	0.8497	0.0000	3.1546	H14-C7-C8-C9 (Torsional)
17.	949	–	964	6.3886	3.4994	20.5484	0.9218	H11-C2-N1-C10 (Torsional)
18.	–	–	979	1.3379	0.7569	2.5847	0.2548	H13-C6-C7-C8 (Torsional)
19.	–	–	986	1.4628	0.8388	0.0000	2.2583	H15-C8-C9 (Bending)
20.	–	–	1006	1.2828	0.7657	0.0000	0.0053	H16-C9-C10 (Bending)
21.	1022	1023	1036	2.2268	1.4093	0.9766	9.8002	H14-C7-C8 (Bending)
22.	1099	–	1055	2.5109	1.6468	19.0134	10.6313	N4-C5 (Stretching)
23.	1126	1128	1151	1.4686	1.1464	9.0329	4.4644	H13-C6-C7 (Bending)
24.	–	–	1168	1.2717	1.0222	1.2999	2.6820	N4-C3 (Stretching)
25.	1203	1207	1239	2.1558	1.9522	2.6919	3.4985	C10-C9 (Stretching)
26.	–	–	1248	2.3333	2.1429	0.3835	6.1811	N1-C10-C9 (Bending)
27.	1283	1287	1292	1.6514	1.6248	0.1047	0.1956	N4-C5-C6 (Bending)
28.	1366	1366	1336	2.9808	3.1365	0.5990	3.6447	H11-C2-N1 (Bending)
29.	–	–	1398	4.5949	5.2975	14.1716	61.2392	N1-C10 (Stretching)
30.	1414	1413	1420	1.7037	2.0241	1.8681	0.3124	C9-C8 (Stretching)
31.	1462	–	1460	2.4502	3.0795	0.4170	105.6932	H12-C3-N4 (Bending)
32.	1493	1494	1510	2.7674	3.7208	1.9524	2.3227	C7-C6-C5 (Bending)
33.	1569	1568	1544	3.3392	4.6937	26.2683	3.3539	C8-C7 (Stretching)
34.	1612	1610	1616	6.8446	10.5335	1.9627	34.3950	N1-C2 (Stretching)
35.	–	–	1617	6.8959	10.6239	0.0637	5.5534	C6-C5 (Stretching)
36.	–	–	1669	5.7791	9.4908	1.6479	5.2710	C7-C6 (Stretching)
37.	1832	–	3155	1.0876	6.3795	7.7613	97.7614	C9-H16 (Stretching)
38.	1939	–	3173	1.0953	6.4973	49.2716	282.1029	C8-H15 (Stretching)
39.	–	2930	3187	1.0864	6.5048	2.8101	59.7188	C7-H14 (Stretching)
40.	–	3015	3200	1.0897	6.5751	8.8162	130.0360	C6-H13 (Stretching)
41.	3032	3059	3213	1.0944	6.6584	11.1516	30.8571	C3-H12 (Stretching)
42.	3420	–	3217	1.0973	6.6936	11.4733	289.9485	C2-H11 (Stretching)

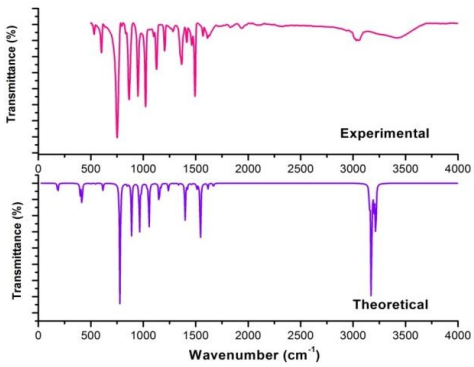

Fig. 2. Comparative experimental and theoretical FTIR spectra of quinoxaline.

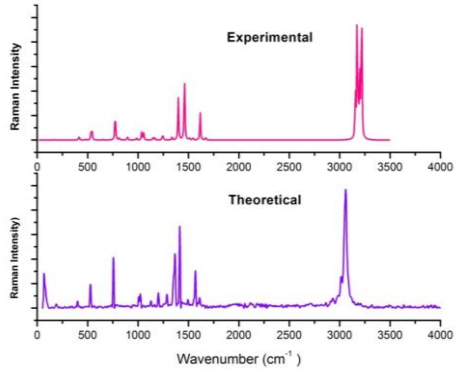

Fig. 3. Comparative experimental and theoretical FT–Raman spectra of quinoxaline.

4.3. *Electronic properties*

For electronic properties, the UV–Vis spectrum was computed using DFT/B3LYP with the 6–31G** basis set, with experimental validation shown in Fig. 4. Table 3 details the theoretically calculated and experimentally observed absorption wavelengths, excitation energies, and oscillator strengths, along with corresponding electronic transitions. The energy from ultraviolet and visible light regions is sufficient to excite outer shell electrons to excited states, shedding light on electron localization and delocalization within the molecule, thereby influencing NLO properties and corrosion inhibition. At 315 nm excited state–1 occur as HOMO→LUMO with 76 % contribution and H–1→ L+1 with 22 % contribution acquiring the excitation energy of 4.5522 eV. At 233 nm excited state–2 occur as H–5→L+5 with 12 %, H–2→LUMO with 65 % and H–2 →L+2 with 22% contributions acquiring the excitation energy of 4.5622 eV. Also, in 204 nm excited state–3 occur as H–1 → LUMO with 62 % and HOMO → L+1 with 32 % contributions having the excitation energy of 4.8873 eV [27].

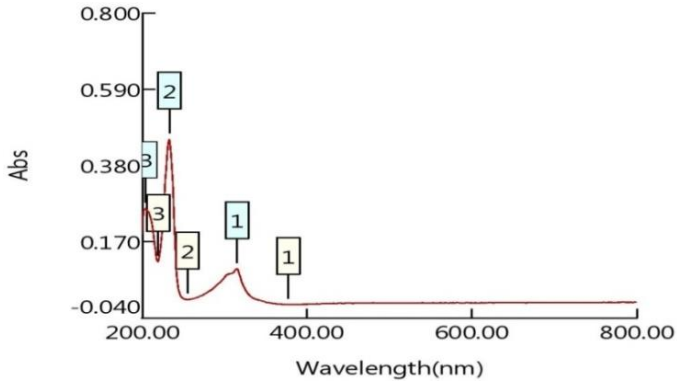

Fig. 4. UV–Vis–NIR absorption spectrum of quinoxaline.

Table 3. The maximum absorbance values of electronic transitions of quinoxaline.

Excited State	Experimental λ_{abs} (nm)	Theoretical λ_{abs} (nm)	Oscillator strength, f	Major contribution	Excitation energy (eV)
1	315	312	0.0733	HOMO→LUMO (76 %) H–1 → L+1 (22 %)	4.5522 eV
2	233	230	0.0064	H–5 → L+5 (12 %) H–2 →LUMO (65 %) H–2 → L+2 (22 %)	4.5622 eV
3	204	202	0.1231	H–1 →LUMO (62 %) HOMO → L+1 (32 %)	4.8873 eV

4.4. *Molecular Electrostatic Potential*

Molecular Electrostatic Potential (MEP) [28] analysis gives insight into the charge distribution, size, shape, and site of chemical reactivity of the molecule. MEP analysis, performed at the B3LYP level with the 6–31G** basis set using Gauss view 5.0, generates three–dimensional color–coded maps representing different molecular electrostatic potentials. The Molecular electrostatic potential and Molecular electronic potential 2D contour map of quinoxaline are given in the Figs. 5 (a) and (b) respectively. Reactive sites susceptible to electrophilic and nucleophilic attacks were identified, with the majority of the quinoxaline map surface displaying neutral potential, interspersed between regions of electrophilic and nucleophilic reactivity. Specifically, negative regions were primarily localized around C6–H13 and C2–N1, while the most positive region was identified around C9–H16, indicating potential sites for nucleophilic attack [29].

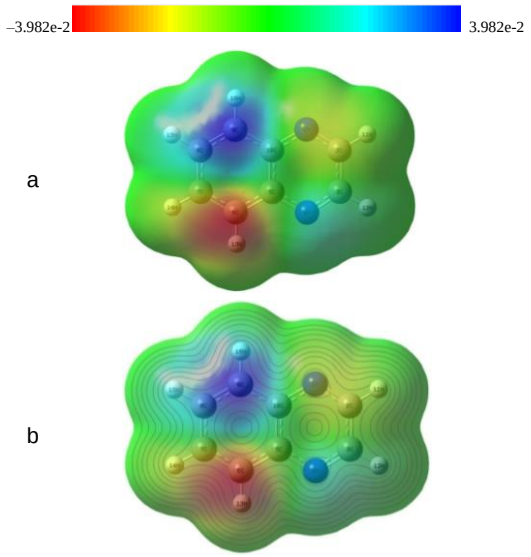

Fig. 5. (a) Molecular electrostatic potential of quinoxaline using Gauss view, (b) Molecular electronic potential 2D contour map of quinoxaline.

4.5. *Frontier molecular orbital*

The chemical and kinetic stabilities of quinoxaline have been assessed through FMO studies. Frontier molecular orbitals, which are spatially delocalized, play a crucial role in molecular interactions. The energy disparity between these molecular orbitals offers valuable insights into the optical, electronic properties, and chemical reactivity of the molecule [30,31]. The filled Highest Occupied Molecular Orbital (HOMO) acts as the electron donor orbital, while the vacant Lowest Unoccupied Molecular Orbital (LUMO) serves as the electron acceptor orbital. The chemical hardness–softness, chemical reactivity kinetic stability, and optical polarizability of a molecule are contingent upon the HOMO–LUMO energy gap. This gap characterizes the molecule's susceptibility to nucleophilic attacks. The following various essential parameters are derived by correlating the HOMO–LUMO values [32].

Chemical hardness (η) and, consequently, chemical softness (S) dictate the level of chemical reactivity. Chemical softness (S) serves as an indicator of the potential toxicity of any pollutants present in the compound [33,34]. The HOMO–LUMO values and associated parameters determined at the B3LYP level with the 6–31G** basis set are presented in Table 3. Fig. 6 illustrates the composition of the HOMO–LUMO frontier molecular orbitals of quinoxaline.

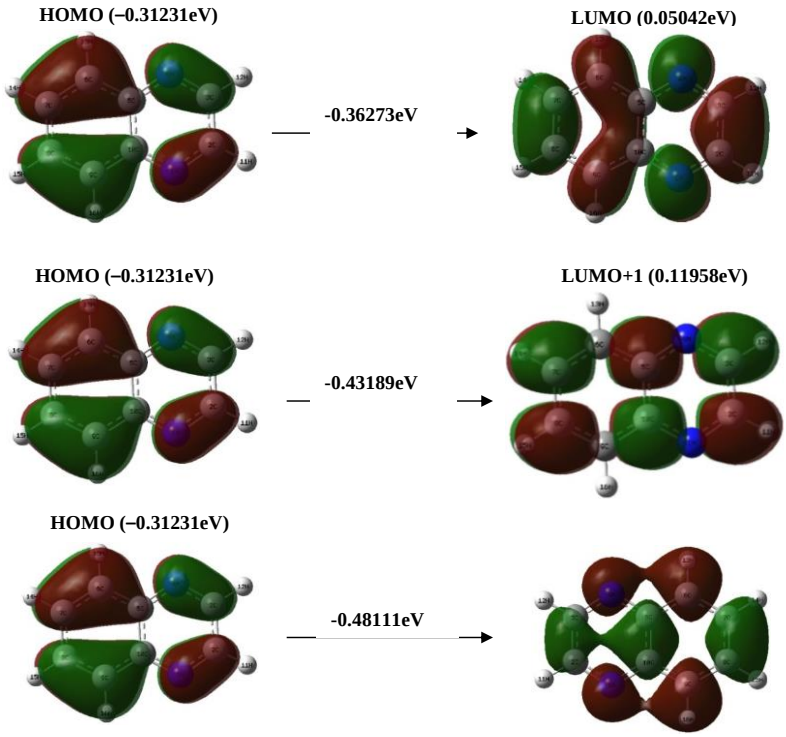

Fig. 6. HOMO–LUMO composition of the frontier molecular orbital of quinoxaline.

These orbitals exhibit mutual attraction due to their energetic correlation. Hard molecules exhibit a large energy gap, whereas soft molecules possess a smaller energy gap. The energy gap of –0.36273 eV for quinoxaline categorizes it into the higher softness category. A low HOMO–LUMO gap indicates heightened reactivity, as electrons require less energy for transfer. The calculated low ionization potential of 0.31231 eV and the low value of electron affinity (–0.05042 eV) indicate increased molecular reactivity with nucleophiles. The electrophilicity index aids in characterizing the compound's biological activity. A small band gap signifies significant interactions between atoms, crucial for electronic and NLO properties [35].

4.6. *NLO analysis*

In pharmacology and drug design, understanding the nonlinear optical (NLO) properties, polarizability, and hyperpolarizability is crucial [36]. The electronic response and NLO activities of a material under exposure to electromagnetic radiation are characterized by parameters such as electric dipole moment (μ), polarizability (α), static polarizability (Δα), and hyperpolarizability (β). These parameters were computed for quinoxaline using finite–field methods with the B3LYP/6–31G** polar basis set and are presented in Table 5.

The total static dipole moment (μ), mean polarizability (α0), anisotropy of polarizability (Δα), and mean first hyperpolarizability (β0) were calculated using the following equations.

The compound exhibits a total dipole moment of 0.337849. The presence of a non–zero dipole moment signifies a difference in electronegativity, resulting in unequal electron sharing among atoms and consequently giving rise to polarizability and hyperpolarizability in the molecule.

The first–order hyperpolarizability (β) of the compound is computed as 156.812200 atomic units. This non–zero dipole moment, coupled with the higher first–order polarizability value, indicates that quinoxaline demonstrates significant nonlinear optical (NLO) activity capable of producing second–order nonlinear effects. It's noteworthy that organic molecules containing nitrogen groups often exhibit enhanced molecular hyperpolarizability [37].

The observed polarizability value suggests that intramolecular interactions primarily stem from π–π* transitions, a characteristic further supported by the presence of conjugated bonds in the compound and UV absorption. Moreover, the smaller HOMO–LUMO energy gap confirms the NLO nature of the compound. Both electronic and NLO characteristics of quinoxaline underscore its biological and pharmaceutical significance.

Table 4. Values of calculated dipole moments, polarizability values and first order hyper-polarizability of quinoxaline molecule.

Components	Parameter	Values Calculated using B3LYP/ 6–31G** basis set in a.u.
Dipole moment components	μ_x	–0.337845
	μ_y	–0.001656
	μ_z	0.000059
Total dipole moment	μ	0.337849
Polarizability components	α_{xx}	145.187058
	α_{yy}	0.261082
	α_{zz}	93.178846
	α_{xy}	–0.000079
	α_{yz}	–0.000446
	α_{xz}	37.447147
Total polarizability	α_0	276.073607
Static polarizability	$\Delta\alpha$	143102.222200
Hyper polarizability components	βxxx	181.829346
	βxxy	1.026568
	βxyy	–9.027555
	βyyy	–0.146985
	βxxz	0.001731
	βxyz	0.001608
	βyyz	0.000211
	βxzz	–15.991607
	βyzz	–0.076245
	βzzz	0.004337
Hyperpolarizability	β	156.812200

4.7. *Molecular docking*

Molecular docking techniques play a pivotal role in characterizing protein–ligand interactions by providing insights into the ligand's bound shape and energetically rating the protein–ligand interaction mechanism. Automated molecular docking was employed to select the optimal in silico conformation for the generated molecules, utilizing the HF basis set of the Gaussian 09W program to refine ligands before docking. Additionally, the online tool PASS (Prediction of Activity Spectra) [38] was utilized to forecast various occurrences related to quinoxaline behavior.

The Protein Data Bank (PDB) [39] contains Thioredoxin h2 (HvTrxh2) in a mixed disulfide complex with the target protein BASI (PDB ID: 2IWT). To predict the ligand–binding site, Q–site Finder was employed to search for probable binding sites of the desired target receptors, typically associated with structured cavities and pockets. Removal of water molecules from crystal packing was done to prevent steric hindrance. Additionally, polar hydrogens missing in the proteins' crystal structure were introduced along with Kollman charges.

The Lamarckian Genetic Algorithm was chosen as the insertion engine, generating populations of 150 individuals with a mutation rate of 0.02 over 10 generations. From 10 conformations, inhibitors with the lowest binding energy scores were selected. To enhance the accuracy the same 10 repetitions were docked and binding affinity values were determined by averaging with the standard deviation.

Quinoxaline possesses 0 rotatable bonds, 6 nonpolar hydrogens and 8 aromatic carbons, with a Gasteiger Charge of –3.0108. Autodock was employed to dock both compounds saved in PDBQT format. On comparing the energy of the 10 docking possibilities the structure displaying the lowest energy considered the best mimic. The ligand–receptor interaction energy was determined to be –3.55 kcal/mol. A hydrogen bond with a strength of 3.0 Å is formed between TRP23 and the nitrogen in quinoxaline, as depicted in the Poseview diagram Fig. 7.

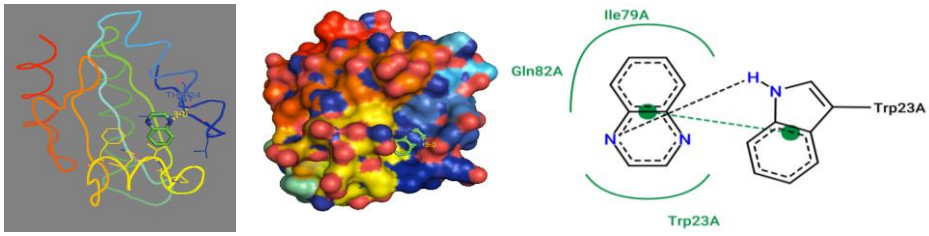

Fig. 7. Poseview diagrams of quinoxaline interaction with protein.

5. Conclusions

The title compound, quinoxaline, underwent experimental confirmation of its characteristics through FTIR, FT–Raman, and UV–Vis–NIR tests. Quantum chemical calculations were conducted at the B3LYP/6–31G** level. PES analysis revealed the presence of a single conformer with an energy of 310.7838 kJ/mol. A comprehensive vibrational analysis of quinoxaline was conducted, encompassing vibrational wave numbers, infrared intensities, and Raman activities. Analysis of HOMO and LUMO, as well as FMO studies, provided insights into the electronic properties, chemical kinetics, hardness and softness, and chemical reactivity of the molecule. Electrophilic, nucleophilic, and radical attack sites were identified through MEP analysis. Additionally, calculations of dipole moment, polarizability, and first–order hyperpolarizability were performed to evaluate the NLO properties of the compound. Molecular docking studies were conducted to elucidate the binding modes, revealing an energy of –3.55 kcal/mol for the ligand–receptor interaction.

References

1. S. Tariq, K. Somakala, and M. Amir, Eur. J. Med. Chem. **143**, 542 (2018). https://doi.org/10.1016/j.ejmech.2017.11.064

2. T. Kaushal, G. Srivastava, A. Sharma, and A. S. Negi, Bioorg. Med. Chem. **27**, 16 (2019). https://doi.org/10.1016/j.bmc.2018.11.021
3. M. Montana, F. Mathias, T. Terme, and P. Vanelle, Eur. J. Med. Chem. **163**, 136 (2019). https://doi.org/10.1016/j.ejmech.2018.11.059
4. X. Hui, J. Desrivot, C. Bories, P. M. Loiseau, X. Franck, R. Hocquemiller, and B. Figadere, Bioorg. Med. Chem. Lett. **16**, 815 (2006). https://doi.org/ 10.1016/j.bmcl.2005.11.025
5. L. E. Seitz, W. J. Suling, and R. C. Reynolds, J. Med. Chem. **45**, 5604 (2002). https://doi.org/10.1021/jm020310n
6. K. Waisser, R. Beckert, M. Slosáfrek, and J. Janota, Pharmazie **52**, 797 (1997).
7. E. Vicente, L. M. Lima, E. Bongard et al., Eur. J. Med. Chem. **43**, 1903 (2008). https://doi.org/10.1016/j.ejmech.2007.11.024
8. A. Carta, M. Loriga, S. Piras, G. Paglietti, P. L. Colla, B. Busonera, G. Collu, and R. Loddo, Med. Chem. **2**, 113 (2006). https://doi.org/10.2174/157340606776056197
9. J. Y. Jaung, **71**, 245 (2006). https://doi.org/10.1016/j.dyepig.2005.07.008
10. K. R. J. Thomas, M. Velusamy, T. Lin Jiann, C. H. Chuen, and Y. T. Tao, Chem. Mater. **17**, 1860 (2005). https://doi.org/10.1021/cm047705a
11. S. Dailey, W. J. Feast, R. J. Peace, I. C. Sage, S. Till, and E. L. Wood, J. Mater. Chem. **11**, 2238 (2001). https://doi.org/10.1039/B104674H
12. S. A. Khan, P. Mullick, S. Pandit, and D. Kaushik, Acta Pol. Pharm. **66**, 169 (2009). http://doi.org/10.1016/j.jep.2005.05.011
13. P. E. M. Siegbahn and T. Borowski, Acc. Chem. Res. **39**, 729 (2006). https://doi.org/10.1021/ar050123u
14. W. Kohn and L. Sham, J. Phys. Rev. **140**, 1133 (1965). https://doi.org/10.1103/PhysRev.140.A1133
15. M. J. Frisch, G. W. Trucks, H. B. Schlegel, G. E. Scuseria, M. A. Robb et al., Gaussian–09, Revision A.01 (Gaussian, Inc., Wallingford, CT, 2009).
16. H. B. Schlegel, J. Comput. Chem. **3**, 214 (1982). https://doi.org/10.1002/jcc.540030212
17. D. Becke, J. Chem. Phys. **98**, 5648 (1993). https://doi.org/10.1063/1.464913
18. C. Lee, W. Yang, and R. G. Parr, Phys. Rev. B **37**, 785 (1988). https://doi.org/10.1103/PhysRevB.37.785
19. M. H. Jamroz, Spectrochim. Acta Part A: Mol. Biomol. Spectrosc. **114**, 220 (2013). https://doi.org/10.1016/j.saa.2013.05.096
20. T. -H. Cha, Chem. Phys. Lett. **765**, 138285 (2021). https://doi.org/10.1016/j.cplett.2020.138285
21. H. G. O. Becker and J. Fleming, Frontier Orbitals and Organic Chemical Reactions (John Wiley, New York, 1978). https://doi.org/10.1002/prac.19783200525
22. G. M. Morris, R. Huey, W. Lindstrom, M. F. Sanner, R. K. Belew et al., J. Comput. Chem. **30**, 2785 (2009). https://doi.org/10.1002/jcc.21256
23. G. Fogarasi, P. Pulay, Annu. Rev. Phys. Chem. **35**, 191 (1984). https://doi.org/10.1146/annurev.pc.35.100184.001203
24. G. Anand, M. Sivasubramanian, I. Manimehan, A. Ruby, R. Abinayashri, and R. K. Asmitha., J. Mol. Struct. **1286**, ID 135586 (2023). https://doi.org/10.1016/j.molstruc.2023.135586.
25. J. Sudhalakshmi, K. Rajathi, J. Sci. Res. **15**, 793 (2023). https://doi.org/10.3329/jsr.v15i3.63522
26. R. Subha1 and N. Ingarsal, J. Sci. Res. 15, 887 (2023). http://doi.org/10.3329/jsr.v15i3.64498
27. E. Akhuseyin, D. Erdener, Karatay et. al., Physica Scripta **98**, 1402 (2023). https://doi.org/10.1088/1402–4896/ace806
28. B. F. Rizwana, S. Muthu, J. C. Prasana, C. S. Abraham, and M. Raja, Chem. Data Collections **17–18**, 236 (2018). https://doi.org/10.1016/j.cdc.2018.09.003
29. M. Raja, R. R. Muhamed, S. Muthu, and M. Suresh, J. Mol. Struct. **1128**, 481 (2017). https://doi.org/10.1016/j.molstruc.2016.09.017
30. C. H. Kaschula, T. J. Egan, R. Hunter, N. Basilico, S. Parapini, D. Taramelli, E. Pasini, and D. Monti, J. Med. Chem. **45**, 3531 (2002). https://doi.org/10.1021/jm020858u

31. N. Muruganantham, R. Sivakumar, N. Anbalagan, V. Gunasekaran, and J. T. Leonard, Biol. Pharm. Bull. **27**, 1683 (2004). https://doi.org/10.1248/bpb.27.1683
32. M. Sivasubramanian, R. R. Saravanan, R. Mendoza-Meroñob, J. Sci. Res. **14**, 545 (2022). http://dx.doi.org/10.3329/jsr.v14i2.57111
33. D. F. V. Lewis, C. Loannides, and D. V. Parke, Xenobiotica **24**, 401 (1994). https://doi.org/10.3109/00498259409043243
34. Z. Zhou and R. G. Parr, J. Am. Chem. Soc. **112**, 5720 (1990). https://doi.org/10.1021/ja00171a007
35. S. L. Dhonnar, N. V. Sadgir, V. A. Adole, and B. S. Jagdale, Adv. J. Chem. A **4**, 220 (2021). https://doi.org/10.22034/AJCA.2021.283003.1254
36. J. R. A. Silva, J. Lameira, and C. N. Alves, Int. J. Quant. Chem. **112**, 3398 (2012). https://doi.org/10.1002/qua.24253
37. H. Sekina and R. J. Bartlett, J. Chem. Phys. Lett. **84**, 2726 (1986). https://doi.org/10.1063/1.450348
38. Way2Drug, Understanding-Biological Interactions, Predictive services, Department for Bioinformatics, Laboratory for Structure Function Based Drug Design, Institute of Biomedical Chemistry (IBMC), Pogodinskaya Str. 10, Bldg.8, Moscow, 119121, Russia. https://www.way2drug.com/passonline (Accessed, 18th May 2024).
39. Worldwide PDB Protein Data Bank, Nature Structural Biology (2003) pp. 1203 -980. https://www.pdb.org (Accessed, 18th May 2024).